ACS APPLIED NANO MATERIALS

www.acsanm.org Article

Visible Light-Responsive Delivery of Two Anticancer Drugs Using Single-Component Fluorescent Organic Nanoparticles

Souvik Ray, Saptarshi Banerjee, Amit Kumar Singh, Mamata Ojha, Arindam Mondal, and N. D. Pradeep Singh*

Cite This: *ACS Appl. Nano Mater.* 2022, 5, 7512−7520 Read Online

ACCESS | Metrics & More | Article Recommendations | Supporting Information

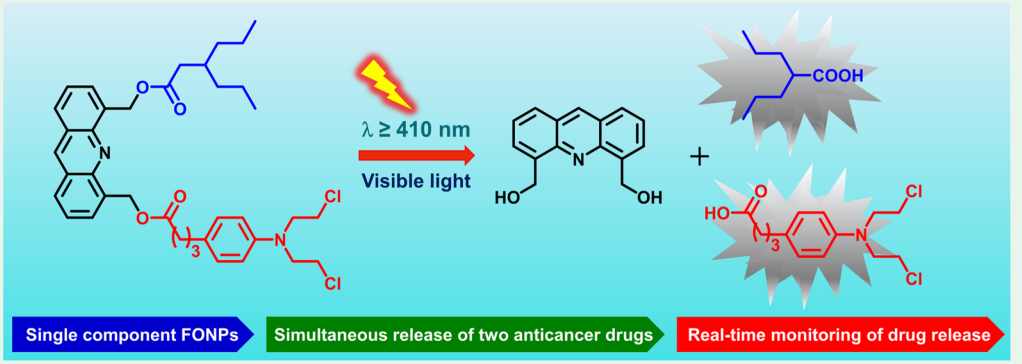

ABSTRACT: Combination therapy is a promising strategy to improve therapeutic efficiency and minimize side effects. So far, the C9-functionalized acridine derivatives were employed as photocages to deliver only one active molecule. Here, we have developed a C4, C5-substituted dual-arm acridine photocage for the first time to release two carboxylic acids and amino acids simultaneously. As a proof of concept, we have constructed a visible light-responsive dual drug delivery system (Acr-Cbl-Vpa) and made it single-component fluorescent organic nanoparticles (NPs) to deliver two anticancer drugs (chlorambucil and valproic acid). Acr-Cbl-Vpa NPs can accumulate inside the cell nucleus, and the planer motif allows the photocage to intercalate with the DNA and maximize the cancer cell killing ability of the drugs. *In vitro* studies with cancerous HeLa cell lines showed that Acr-Cbl-Vpa NPs displayed improved anticancer efficacy and real-time fluorescence monitoring of the drug release.

KEYWORDS: *combination therapy, dual-arm acridine, photocage, FONPs, nuclear-targeted delivery, anticancer drug*

INTRODUCTION

Photoremovable protecting groups or photocages enable the release of active molecules with high spatiotemporal control.[1] Therefore, photocages are gaining tremendous popularity for several biological and material applications.[2−5] Recently, photocages with dual release capacity have become highly required in therapeutics, especially in delivering two anticancer drugs.[6,7] A combination or cocktail chemotherapy is advantageous over single drug-based chemotherapy as it increases the therapeutic efficacy by minimizing the multidrug resistance of the cancer cells.[8−11] For this purpose, different dual-arm photocages were developed using carbazole, *o*-nitrobenzyl, and bimane chromophores.[12−14] However, poor aqueous solubility and low photocytotoxicity reduce the anticancer efficacy of these photocages. Moreover, these photocages could not show real-time fluorescence color change during photolysis. Therefore, there is an actual demand for building a dual-arm photocage with good aqueous solubility, high biocompatibility, enhanced photocytotoxicity, and real-time monitoring ability.

In this regard, acridine is a potential bioactive molecule, and many of its derivatives are extensively studied for their antibacterial, antimalarial, and anticancer activities.[15−19] Besides, the planer structure of acridine allows it to intercalate with DNA and inhibit the topoisomerase-II enzyme.[20,21] These findings provided the opportunity to design acridine-based photocages for targeted control release of anticancer drugs. Zhuang and co-workers first introduced 9-hydroxymethylacridine chromophore as a photocage for different alcohols.[22] Furthermore, our group and Piloto et al. employed the same C9-functionalized acridine photocage to release neurotransmitter amino acids and carboxylic acids.[23,24] However, this C9-functionalized acridine photocage can release only one active

Received: April 8, 2022
Accepted: April 29, 2022
Published: May 10, 2022

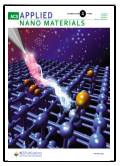

https://doi.org/10.1021/acsanm.2c01515
ACS Appl. Nano Mater. 2022, 5, 7512−7520

molecule, restricting its application in combination therapy. Therefore, we designed a C4- and C5-functionalized acridine (acridine-4,5-diyldimethanol) photocage for the first time to release two (same and different) carboxylic acids and amino acids simultaneously.

On the other hand, light-responsive fluorescent organic nanoparticles (FONPs) have received much attention in drug delivery.[25] These single-component FONPs act as a photocage and a nanocarrier for delivering anticancer drugs. Interestingly, the dispersion of the photocage NPs in water makes them very useful for their applications in biological media. Previously, our group developed light-responsive FONPs as anticancer drug delivery systems using photocages, namely, perylene-3-ylmethyl, acridin-9-methyl, and *p*-hydroxyphenacyl.[26−29] This encouraged us to build an acridine-based single-component nanocarrier that simultaneously delivers two different anticancer drugs (Figure 1).

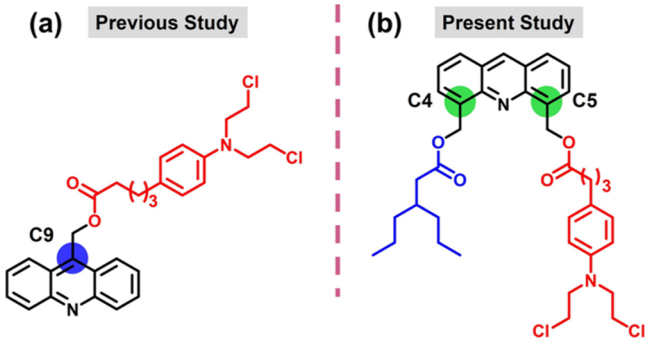

Figure 1. (a) Jana and co-workers' C9-functionalized acridine photocage for nuclear-targeted drug delivery and (b) C4, C5-substituted dual-arm acridine photocage for simultaneous release of two anticancer drugs.

In this study, we have utilized acridine-4,5-diyldimethanol to construct dual-arm fluorescent photocages to release carboxylic acids and amino acids. Our designed photocages are (i) easy to synthesize, (ii) encapsulate two (same and different) carboxylic and amino acids, and (iii) show a clean photo-deprotection reaction.

Furthermore, we have applied acridine-4,5-diyldimethanol as a nanocarrier to deliver two anticancer drugs. For this purpose, we have attached chlorambucil (a well-known DNA alkylating agent) and valproic acid (a histone deacetylase inhibitor[30]) with acridine-4,5-diyldimethanol and made them as single-component fluorescent organic NPs (Acr-Cbl-Vpa) using a reprecipitation technique.[31,32] Our newly designed nano-drug delivery system shows a distinct fluorescence color change from green to blue upon photoinduced uncaging (Scheme 1). We have also performed the *in vitro* cellular imaging and cytotoxicity assay to check the biocompatibility and anticancer activity of the nano-drug delivery system.

RESULTS AND DISCUSSION

The dual-arm acridine photocages were synthesized, as shown in Scheme 2. Acridine-4,5-diyldimethanol (**2**) was prepared according to the literature report.[33] The identical dual-arm caged esters (**3a−e**) were synthesized by an EDC coupling reaction between the alcohol (**2**) and the corresponding carboxylic acids or N-protected amino acids. The dual different arm caged ester (**5a**) was synthesized in two steps; first, *p*-anisic acid was treated with compound **2** to get (5-(hydroxymethyl)acridin-4-yl)methyl-4-methoxybenzoate (**4a**), which was further coupled with *p*-toluic acid using EDC.HCl to obtain **5a**. We characterized all the caged esters (**3a−e**, **5a**) by ^{1}H NMR, ^{13}C NMR, and HRMS (see the Supporting Information, Pages S2−S17).

The absorption and emission spectra of **3a−e** and **5a** were recorded in a 1×10^{-5} M acetonitrile solution (Table S1). The normalized absorption and emission spectra of **3a** are shown in Figure 2. We noticed that compound **3a** shows a sharp peak at around 357 nm in the absorption spectrum and maximum emission at 449 nm, giving a Stokes shift of 92 nm. The absorption maxima, molar absorptivity, emission maxima, Stokes shifts, and fluorescence quantum yield of **3a−e** and **5a** are provided in Table S1. The fluorescence quantum yield (Φ_f) of the acridine photocages was calculated (see the Supporting Information) using quinine sulfate (Φ_f = 0.54).[34]

The photouncaging abilities of all the caged esters (**3a−e**, **5a**) were analyzed. We irradiated the argon-purged solution of all the caged esters (1.0×10^{-5} M) individually in a 3:7 v/v acetonitrile/water mixture using a Hg lamp (125 W; $I_0 = 3.7 \times 10^{17}$quanta s^{-1}; $\lambda \geq 365$ nm).

Photolysis of **3a−e**, **5a** for 110 min resulted in 83−88% release of the analogous carboxylic acids and amino acids with good quantum yield (0.044−0.047), as shown in Table 1. We calculated the photochemical quantum yield (Φ_p) using ferrioxalate actinometry (see the Supporting Information).[35]

The course of photorelease of **3a** (as a representative example) was monitored using RP-HPLC and fluorescence spectroscopy (Figure 3a,b). We carried out the RP-HPLC using a binary mixture of ACN/H_2O (9:1, v/v) as the mobile phase. The RP-HPLC chromatogram (Figure 3a) shows a

Scheme 1. Schematic Representation for the Fabrication of Acr-Cbl-Vpa NPs and the Anticancer Drug Release Inside the Cell

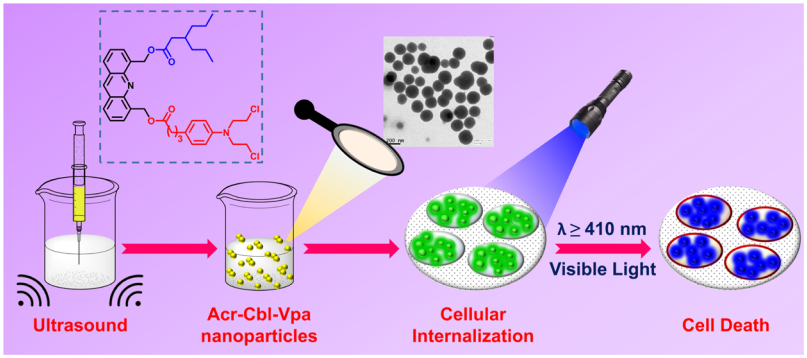

https://doi.org/10.1021/acsanm.2c01515
ACS Appl. Nano Mater. 2022, 5, 7512−7520

Scheme 2. Synthesis of the C4, C5-Substituted Dual-Arm Acridine Caged Esters. Reagents and Conditions: (a) (i) Bromomethyl Methyl Ether, H_2SO_4, 50 °C, 12 h, 65%; (ii) $CaCO_3$, H_2O, Dioxane, 140 °C, 4 h, 91%; and (iii) EDC·HCl, DMAP, R_1COOH (2 equiv), DCM, 0 °C-rt, 6 h; and (b) (i) EDC.HCl, DMAP, R_2COOH (1 equiv), DCM, 0 °C, 2 h, 60% and (ii) EDC·HCl, DMAP, R_3COOH (1 equiv), DCM, rt, 6 h

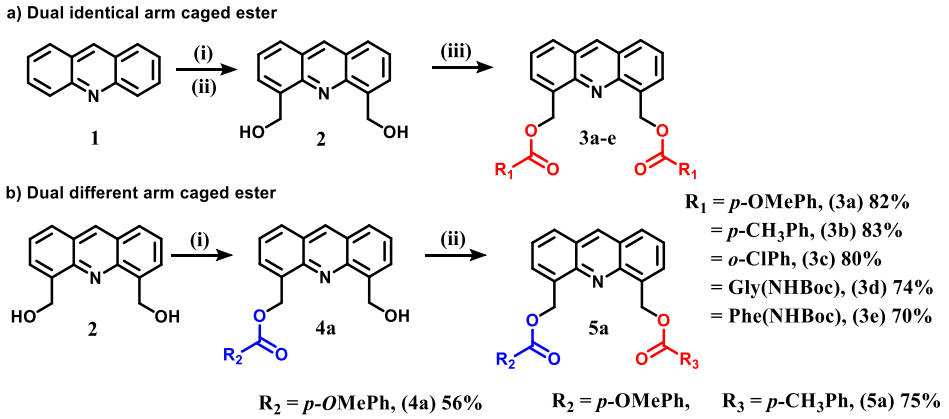

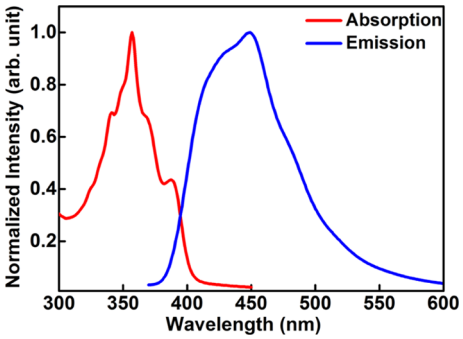

Figure 2. Absorption and emission spectra of compound **3a**.

Table 1. Photochemical Data Set for 3a–e and 5a

Caged Ester	Carboxylic Acid[a]	Deprotection Yield[b] %	Quantum Yield[c] (ϕ_P)
3a	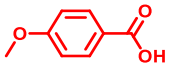	86	0.047
3b	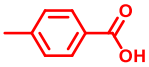	88	0.046
3c	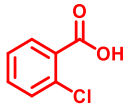	87	0.046
3d	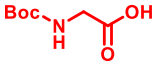	84	0.044
3e	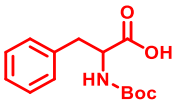	83	0.045
5a	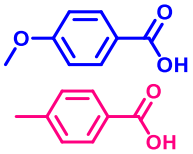	87 85	0.025 0.023

[a]Caged carboxylic acids and amino acids. [b]Percentage of deprotected acid (obtained by RP-HPLC) from the caged ester after irradiation ($\lambda \geq 365$ nm). [c]Photochemical quantum yield of photorelease (error limit within ±10%).

steady decrease of the peak **a** at the retention time (t_R) of 4.8 min with the increasing irradiation time, which indicates the photodecomposition of **3a**. In addition, two new peaks, **c** and **d**, gradually arise at t_R 3.1 min and 2.0 min, respectively, which correspond to the released photoproduct acridine-4,5-diyldimethanol and the uncaged *p*-anisic acid, respectively. The peak **b** at t_R 3.5 min, initially found overlapping with peak **c**, gradually decreases as photolysis time increases. This peak corresponds to the intermediate (5-(hydroxymethyl)acridin-4-yl)methyl-4-methoxybenzoate (**4a**), which decomposes to produce the final photoproduct acridine-4,5-diyldimethanol (peak **c**) and *p*-anisic acid (peak **d**). The intermediate (5-(hydroxymethyl)acridin-4-yl)methyl-4-methoxybenzoate, final photoproduct (acridine-4,5-diyldimethanol), and released *p*-anisic acid were isolated. The final photoproduct (acridine-4,5-diyldimethanol) was characterized by ^{1}H NMR and HRMS (Figures S19 and S20).

Another set of experiments was carried out to monitor the photolysis of **3a** by fluorescence spectroscopy. A degassed solution of caged ester **3a** (1.0×10^{-6} M) in acetonitrile/water (1:9 v/v) was irradiated [incident photon intensity (I_0) = 3.7×10^{17}quanta s^{-1}] for 40 min. Then, the fluorescence spectrum was recorded at different time intervals between 0 and 40 min (Figure 3b). We observed a gradual hypsochromic shift in emission maxima during the photolysis of **3a**. This blue-shifted emission was attributed to the formation of the photoproduct acridine-4,5-diyldimethanol (Figure S21).

From this photolysis data (obtained by RP-HPLC), we observed that the photodissociation of **3a** followed first-order kinetics with a rate constant of 2.98×10^{-4} s^{-1} (Figure 4a). Furthermore, we did a light on–off experiment to show the precise control over the photorelease. We periodically monitored the photoproduct formation from **3a** under light and dark conditions, and the HPLC data indicated that only light induces the photorelease (Figure 4b).

Based on the photochemical studies and earlier literature reports,[36,37] we have suggested a possible mechanism for the photolysis of acridine caged ester **3a** in Scheme 3. Initially, **3a** gets excited to the singlet excited state (S_1) (^{1}[**3a**]*), which then undergoes a heterolytic C–O bond cleavage at the benzylic position at either C4 or C5 to produce an ion pair. Upon solvent capture, the tight ion pair releases one equivalent of *p*-anisic acid and forms (5-(hydroxymethyl)acridin-4-

https://doi.org/10.1021/acsanm.2c01515
ACS Appl. Nano Mater. 2022, 5, 7512–7520

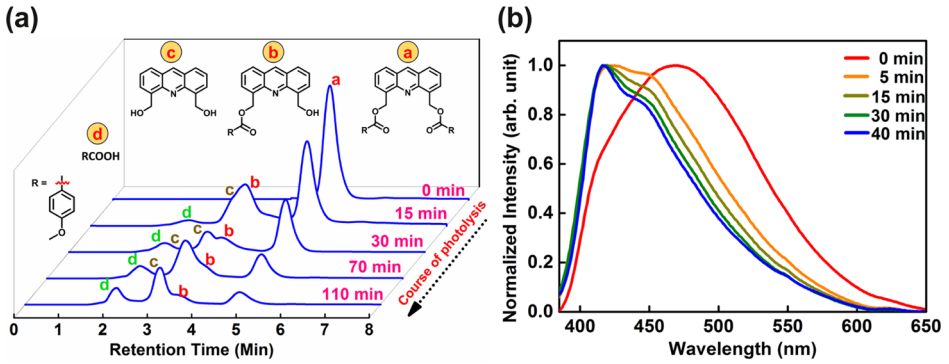

Figure 3. (a) Overlay of HPLC chromatograms of the caged ester **3a** at the different course of photolysis; (b) fluorescence monitoring of the photolysis of **3a**. The red line designates the fluorescence spectrum of **3a** at 0 min; the blue line designates the fluorescence spectrum of **3a** after 40 min of light irradiation; and the orange, dark yellow, and dark green lines represent the fluorescence spectra of **3a** at different intervals (5, 15, and 30 min, respectively) of light irradiation.

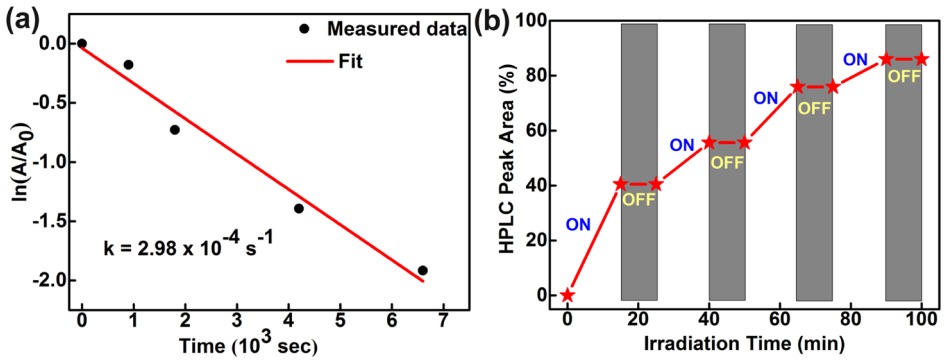

Figure 4. (a) Rate constant of photouncaging of caged ester **3a** (Obtained from HPLC); (b) temporal control over the photouncaging of **3a**. The "ON" state indicates the active stage of photochemical reaction in the presence of light, and the "OFF" state indicates the dark step; the reaction is stopped in the absence of light.

Scheme 3. Possible Photorelease Pathway of Caged Ester 3a

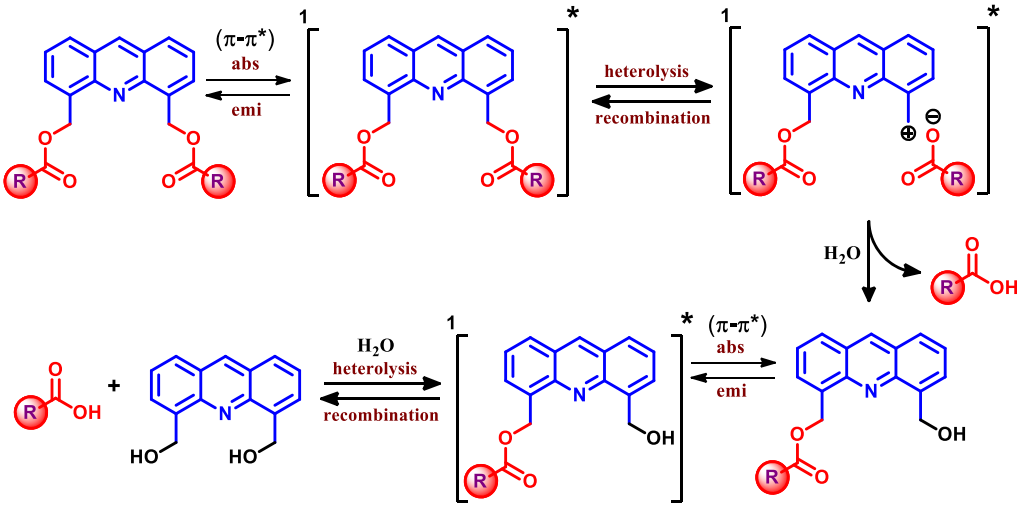

yl)methyl-4-methoxybenzoate (**4a**). Then, compound **4a** again gets excited to S_1 (^{1}[**4a**]*) and produces another equivalent of *p*-anisic acid along with the final photoproduct (acridine-4,5-diyldimethanol).

After a successful demonstration of acridine-4,5-diyldimethanol as a dual-arm photocage, we were encouraged to construct a single-component nano-photocage to release two anticancer drugs. First, we synthesized the dual drug conjugate Acr-Cbl-Vpa (**9**) by caging chlorambucil on one arm and valproic acid on another arm, as illustrated in Scheme 4. The drug conjugate **9** was characterized by NMR (^{1}H and ^{13}C) and HRMS (Figure S9 and S18).

Acr-Cbl-Vpa NPs were prepared by a reprecipitation method, that is, slow addition of the dilute solution of Acr-Cbl-Vpa (25 μL, 1 mM in THF) into water (25 mL) for 30 min using an ultrasonic bath sonicator (Scheme S1). The shape and size of the resulting Acr-Cbl-Vpa NPs were determined by TEM and DLS, respectively. We observed

https://doi.org/10.1021/acsanm.2c01515
ACS Appl. Nano Mater. 2022, 5, 7512−7520

Scheme 4. Synthesis of Photoresponsive Dual Drug Conjugate Acr-Cbl-Vpa

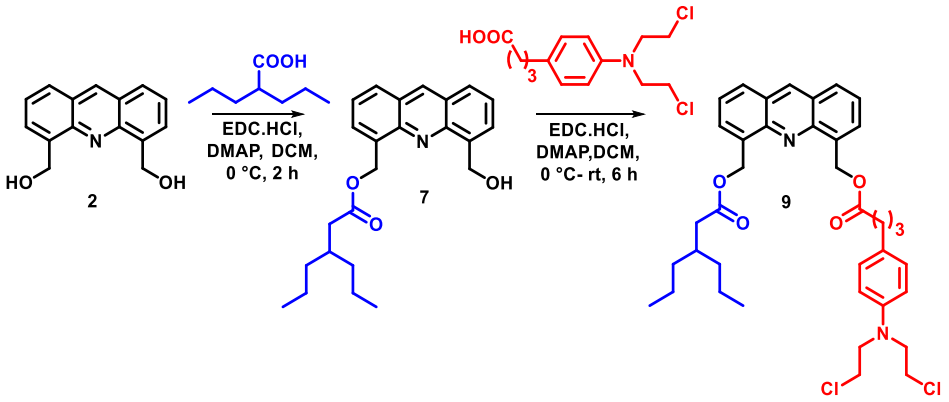

that the NPs were formed in a bulbous shape with an average size of 92 nm (Figures 5a,b and S22). These NPs can effectively penetrate and accumulate inside the cancerous cells due to the EPR (enhanced permeability and retention) effect.[38]

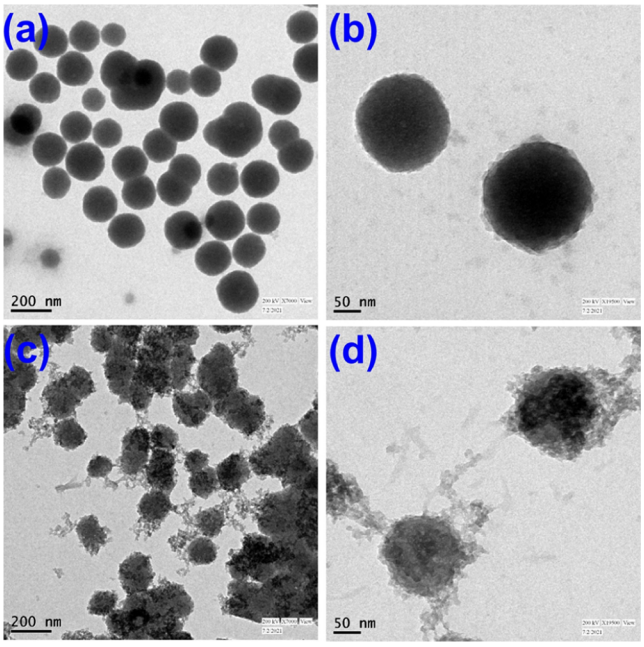

Figure 5. (a−d) TEM images of Acr-Cbl-Vpa NPs (a,b) before photolysis and (c,d) after photolysis.

The absorption and emission spectra (Figures 6a,b and S23) of Acr-Cbl-Vpa NPs show a broad absorption peak at 368 nm and a wide emission band around 528 nm, respectively. Next, the drug release ability of Acr-Cbl-Vpa NPs was evaluated using RP-HPLC. A 25 mL of aqueous suspension (1×10^{-6} M) of Acr-Cbl-Vpa NPs was exposed to visible light. The photolysis was monitored by RP-HPLC (Figure S25). After 40 min of light irradiation, almost all Acr-Cbl-Vpa NPs were consumed (monitored by the HPLC peak area). Again, we have also investigated the hydrolytic stability of Acr-Cbl-Vpa NPs. An aqueous dispersion of Acr-Cbl-Vpa was stored at room temperature under dark conditions for 2 days, which resulted in no significant drug release (Table S2). TEM images (Figure S24) also showed that Acr-Cbl-Vpa NPs were stable under dark conditions.

The Acr-Cbl-Vpa nano-drug delivery system also exhibited the real-time monitoring ability during photolysis (Figure 7a). An aqueous suspension of Acr-Cbl-Vpa NPs was irradiated using visible light ($\lambda \geq 410$ nm), and the emission spectra were recorded (with an excitation wavelength of 370 nm) at a regular interval of 5 min between 0 and 40 min. The initial emission maxima at 528 nm started decreasing gradually, and a new emission band appeared at 426 nm. After 40 min of irradiation, the peak at 528 nm almost vanished, which suggested the completion of the reaction. The newly formed peak at 426 nm was attributed to the formation of the photoproduct (acridine-4,5-diyldimethanol) (Figure S21). The decrease in the emission maxima was due to degeneration of the aggregated state in the NPs during photolysis (Figure 5c,d). The deformed NPs could no longer give the red-shifted broad emission signal at 528 nm; instead, a sharp emission maximum was observed at 426 nm.

Acridine derivatives are well-known DNA intercalators. We have performed the ethidium bromide (EtBr) displacement assay to establish the DNA binding of Acr-Cbl-Vpa NPs. In the beginning, the fluorescence intensity of EtBr was enhanced after intercalation with the DNA (plasmid). However, with the gradual addition of Acr-Cbl-Vpa NPs to EtBr-DNA, the fluorescence intensity of EtBr started decreasing (Figure 7b).

This observation indicates that Acr-Cbl-Vpa NPs preferred to intercalate with DNA. The quenching of EtBr-bound DNA by Acr-Cbl-Vpa NPs fitted well with the linear Stern−Volmer equation (Figure S26).

Cell imaging studies revealed the cellular internalization of Acr-Cbl-Vpa NPs within the cancerous HeLa cells. Cells were incubated with Acr-Cbl-Vpa NPs for 4 h and imaged with a fluorescence microscope (Figure 8ii-iii). The treated cells showed fluorescence signals from the nano aggregates inside the cell, confirming cellular uptake. Furthermore, cell nuclei were counter-stained with propidium iodide. We noted a significant overlap of a diffused green fluorescence signal from the NPs with the red propidium iodide signal, indicating a free distribution of the particles inside the cell cytoplasm and nucleus (Figure 8iv). Real-time monitoring of drug release by our Acr-Cbl-Vpa NPs was followed by fluorescence microscopy. Initially, the cells exhibited green fluorescence due to the internalization of Acr-Cbl-Vpa NPs. A weak fluorescence signal was observed in the blue channel, probably due to minimal cleavage of the photocage. After 30 min of exposure to light ($\lambda \geq 410$ nm), the cells showed morphological changes, including cell shrinkage and cytoplasmic blebbing and significant fluorescence enhancement in the blue channel, suggesting

https://doi.org/10.1021/acsanm.2c01515
ACS Appl. Nano Mater. 2022, 5, 7512−7520

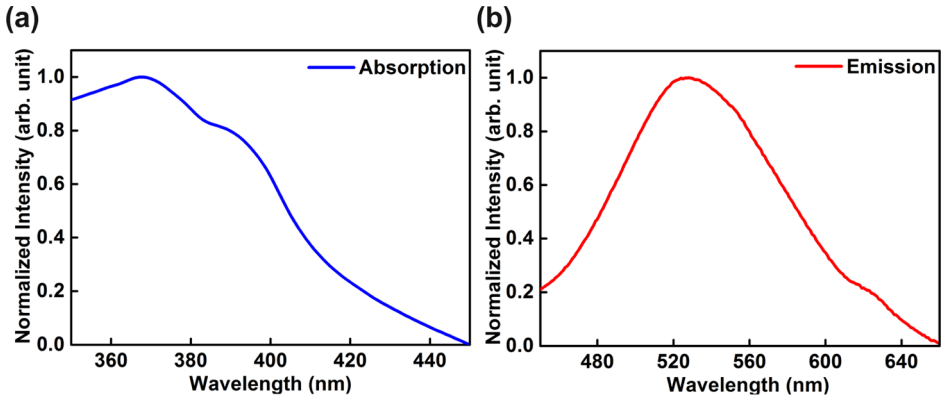

Figure 6. Normalized (a) absorption and (b) emission spectra of Acr-Cbl-Vpa NPs.

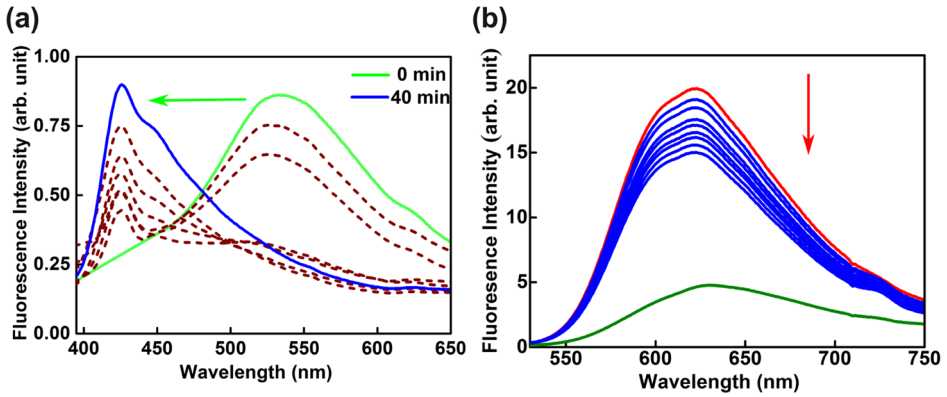

Figure 7. (a) Real-time monitoring by emission spectra of the Acr-Cbl-Vpa NPs during photolysis ($\lambda \geq 410$ nm). (b) Quenching of fluorescence spectrum of EtBr−DNA with gradual addition of Acr-Cbl-Vpa NPs. The green line shows the fluorescence spectra of EtBr, the red line shows the fluorescence spectrum of EtBr-DNA, and the blue lines indicate the quenching of fluorescence upon the addition of Acr-Cbl-Vpa NPs.

the photorelease of the drugs (chlorambucil and valproic acid). A green fluorescence signal in the irradiated cells was observed due to the uncleaved Acr-Cbl-Vpa NPs. The overall fluorescence signal was enhanced in irradiated shrunk cells due to an increased local concentration of the NPs.

Subsequently, we have evaluated the *in vitro* cytotoxicity of Acr-Cbl-Vpa NPs using an MTT assay (Figure 9a,b). Before photolysis, the cell viability remained above 90% up to 25 μM of Acr-Cbl-Vpa NPs. Cellular toxicity was observed without light irradiation at 50 μM concentration of Acr-Cbl-Vpa ~30%. Upon light irradiation, Acr-Cbl-Vpa NP-incubated cells exhibited almost twofold cytotoxicity (EC_{50} = 12.59 μM) compared to free chlorambucil (EC_{50} = 20.23 μM). Free valproic acid is a histone deacetylase (HDAC) inhibitor and did not show any significant cytotoxicity at the investigated concentrations, similar to previous reports.[39] Interestingly, the combination of valproic acid with chlorambucil in the nano-drug delivery system showed enhanced cytotoxicity against cancerous HeLa cells compared to the individual free drugs. This suggests a synergistic effect of valproic acid upon chlorambucil, similar to previous reports.[40] Thus, Acr-Cbl-Vpa NPs serve as a multipurpose drug delivery system due to efficient cellular uptake and the combined effect of chlorambucil and valproic acid inside the cancer cell.

CONCLUSIONS

As a final remark, we have constructed a C4- and C5-functionalized dual-arm acridine photocage, which can release different carboxylic acids and amino acids. Then, we have utilized our photocage as single-component photoresponsive fluorescent organic NPs (Acr-Cbl-Vpa) to simultaneously release two anticancer drugs (chlorambucil and valproic acid). Acr-Cbl-Vpa NPs manifested real-time information through a green to blue fluorescence color change during drug release. Excellent cellular uptake capability, appreciable biocompatibility, and great spatiotemporal control over drug release make Acr-Cbl-Vpa an excellent nano-vehicle for photoresponsive drug delivery.

EXPERIMENTAL SECTION

Synthesis of Acr-Cbl-Vpa NPs. A 1×10^{-3} M THF stock solution was prepared for Acr-Cbl-Vpa. Then, 25 μL stock solutions were taken via a 100 μL syringe and added dropwise into 25 mL of water in a glass beaker inside an ultrasonic bath sonicator. The addition was continued for 30 min. Next, removal of THF from the solution by argon purging gave a 1×10^{-6} M aqueous suspension of Acr-Cbl-Vpa NPs.

Photolysis of Acr-Cbl-Vpa NPs. A 25 mL aqueous suspension (1×10^{-6} M) of Acr-Cbl-Vpa NPs was exposed to light ($\lambda \geq 410$ nm) by a 125 W mercury lamp. 1 M $NaNO_2$ solution was used as a filter. The photolysis was examined by RP-HPLC.

Cell Lines. We obtained the HeLa cell lines from the National Centre for Cell Science (NCCS), India. The cell line was kept in Dulbecco's modified Eagle's medium (DMEM) (Gibco) media along with 10% fetal bovine serum, 20 mM L-glutamine (Gibco), and 1% penicillin−streptomycin (Gibco) in a humidified incubator (Thermo Fisher Scientific) at a temperature of 37 °C in the presence of 5% CO_2.

Real-Time Fluorescence Monitoring of Acr-Cbl-Vpa NPs inside HeLa Cells. The cancerous HeLa cell line was used to study

https://doi.org/10.1021/acsanm.2c01515
ACS Appl. Nano Mater. 2022, 5, 7512−7520

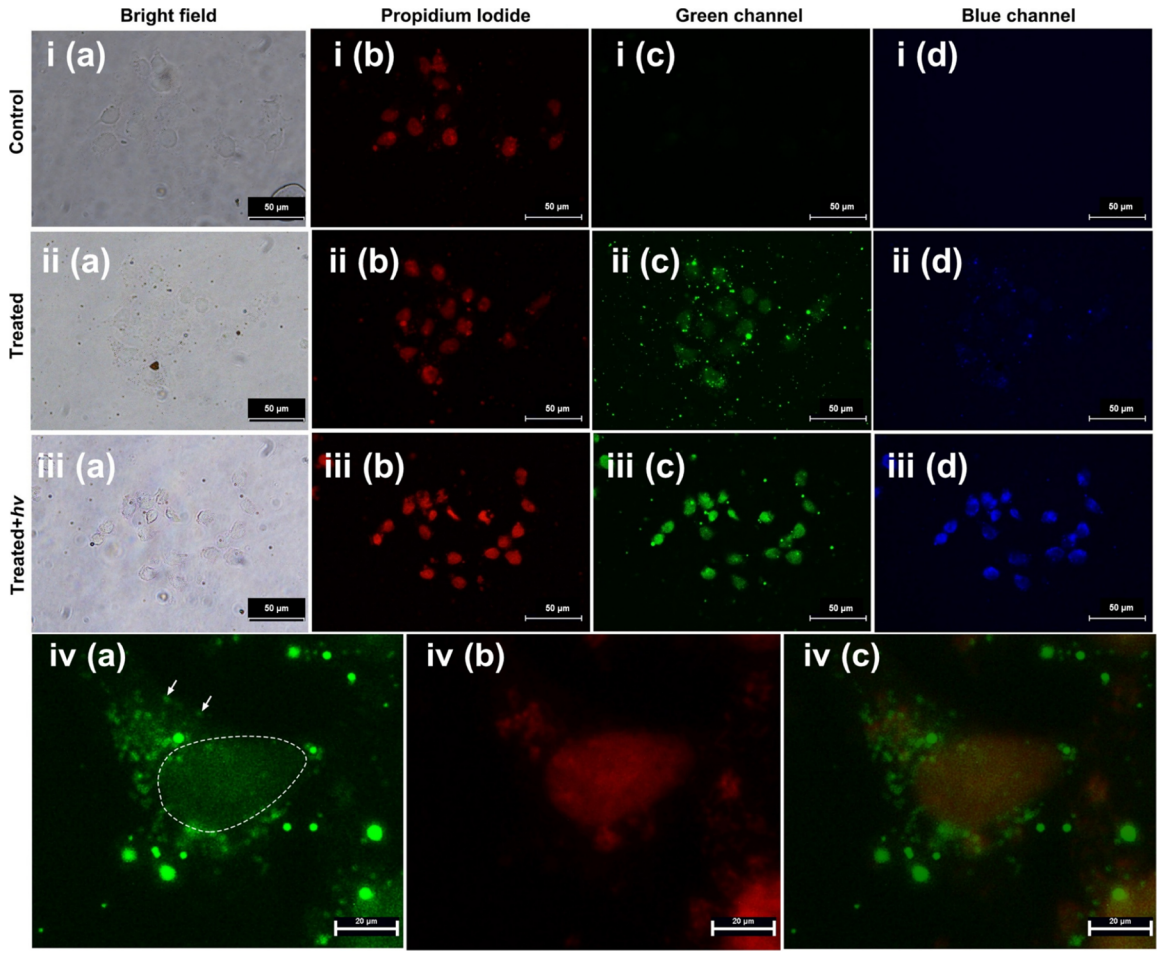

Figure 8. Bright-field and fluorescence images of HeLa cells: (i) control experiment (without Acr-Cbl-Vpa NPs). (ii–iii) Incubation with 50 μM Acr-Cbl-Vpa NPs for 4 h following fixation of cells and staining by PI (propidium iodide), (a) bright-field image of cells, (b) staining of the nucleus by PI, (c) uptake of Acr-Cbl-Vpa NPs in the green channel, and (d) uptake of Acr-Cbl-Vpa NPs in the blue channel. Scale bar = 50 μM. (iv) Internalization of Acr-Cbl-Vpa NPs inside the cell. (a,b) Distribution of Acr-Cbl-Vpa NPs in the cell (the white line marks the cell's nucleus, and the white arrow shows the cytoplasmic aggregates). (c) Overlay of PI stained nucleus and Acr-Cbl-Vpa NPs inside the cell. Scale bar = 20 μM.

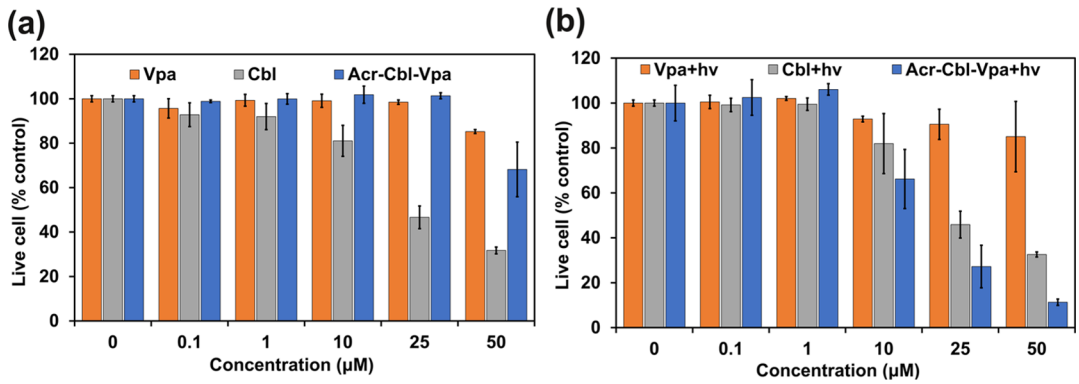

Figure 9. (a,b) Cell viability studies of Acr-Cbl-Vpa NPs, chlorambucil, and valproic acid in HeLa cells: (a) before light exposure and (b) after light exposure. All the values are presented as mean ± SD.

the uptake of the Acr-Cbl-Vpa NPs. 1×10^5 cells were seeded in each well of a 12 well plate. 20 h post-incubation, cells were treated with 100 μM of the Acr-Cbl-Vpa NPs and incubated for 4 h. Cells were either exposed to visible light for 30 min or kept under dark conditions in the incubator after incubation. Following that, cells were fixed with 3% formaldehyde, and nucleus staining was done with propidium iodide and RNase A treatment. Images were taken with a Leica fluorescence microscope.

***In Vitro* Cell Viability Assay.** Anticancer efficacy was tested on the cancerous HeLa cell line. 10 000 cells were seeded in 96 well plates and cultured in DMEM with fetal bovine serum and penicillin–streptomycin, at 37 °C in the presence of 5% CO_2. After 20 h of the incubation period, cells were treated with different concentrations of Acr-Cbl-Vpa NPs. 4 h after incubation with the NPs, the cells were either exposed to visible light for 30 min or kept in the dark. Then, the cell viability was measured using a MTT (3-(4,5-dimethylthiazol-2-yl)-2,5-diphenylte-trazolium bromide) assay.

https://doi.org/10.1021/acsanm.2c01515
ACS Appl. Nano Mater. 2022, 5, 7512–7520

■ ASSOCIATED CONTENT

Supporting Information

The Supporting Information is available free of charge at https://pubs.acs.org/doi/10.1021/acsanm.2c01515.

Synthesis details, characterization data, and other experimental details. FAIR Data is available as the supporting information for Publication and includes the primary NMR FID files for compounds (PDF)

■ AUTHOR INFORMATION

Corresponding Author

N. D. Pradeep Singh − *Department of Chemistry, Indian Institute of Technology Kharagpur, Kharagpur, West Bengal 721302, India;* orcid.org/0000-0001-6806-9774; Email: ndpradeep@chem.iitkgp.ac.in

Authors

Souvik Ray − *Department of Chemistry, Indian Institute of Technology Kharagpur, Kharagpur, West Bengal 721302, India*

Saptarshi Banerjee − *School of Bioscience, Indian Institute of Technology Kharagpur, Kharagpur, West Bengal 721302, India*

Amit Kumar Singh − *Department of Chemistry, Indian Institute of Technology Kharagpur, Kharagpur, West Bengal 721302, India*

Mamata Ojha − *Department of Chemistry, Indian Institute of Technology Kharagpur, Kharagpur, West Bengal 721302, India*

Arindam Mondal − *School of Bioscience, Indian Institute of Technology Kharagpur, Kharagpur, West Bengal 721302, India*

Complete contact information is available at: https://pubs.acs.org/10.1021/acsanm.2c01515

Notes

The authors declare no competing financial interest.

■ ACKNOWLEDGMENTS

We thank DST SERB (grant no. DIA/2018/000019) for financial support and DST-FIST for 600 and 400 MHz NMR instruments. S.R. is thankful to IIT Kharagpur for the fellowship. S.B. thanks CSIR for the fellowship (CSIR file no: 09/081(1301)/2017-EMR-I).

■ REFERENCES

(1) Klán, P.; Šolomek, T.; Bochet, C. G.; Blanc, A.; Givens, R.; Rubina, M.; Popik, V.; Kostikov, A.; Wirz, J. Photoremovable Protecting Groups in Chemistry and Biology: Reaction Mechanisms and Efficacy. *Chem. Rev.* **2013**, *113*, 119−191.

(2) Weinstain, R.; Slanina, T.; Kand, D.; Klán, P. Visible-to-NIR-Light Activated Release: From Small Molecules to Nanomaterials. *Chem. Rev.* **2020**, *120*, 13135−13272.

(3) Pelliccioli, A. P.; Wirz, J. Photoremovable Protecting Groups: Reaction Mechanisms and Applications. *Photochem. Photobiol. Sci.* **2002**, *1*, 441−458.

(4) Kand, D.; Liu, P.; Navarro, M. X.; Fischer, L. J.; Rousso-Noori, L.; Friedmann-Morvinski, D.; Winter, A. H.; Miller, E. W.; Weinstain, R. Water-Soluble BODIPY Photocages with Tunable Cellular Localization. *J. Am. Chem. Soc.* **2020**, *142*, 4970−4974.

(5) Zhao, H.; Sterner, E. S.; Coughlin, E. B.; Theato, P. O-Nitrobenzyl Alcohol Derivatives: Opportunities in Polymer and Materials Science. *Macromolecules* **2012**, *45*, 1723−1736.

(6) Xiao, W.; Zeng, X.; Lin, H.; Han, K.; Jia, H.-Z.; Zhang, X.-Z. Dual stimuli-responsive multidrug delivery system for the individually controlled release of anticancer drugs. *Chem. Commun.* **2015**, *51*, 1475−1478.

(7) Liu, J.; Yang, G.; Zhu, W.; Dong, Z.; Yang, Y.; Chao, Y.; Liu, Z. Light-controlled drug release from singlet-oxygen sensitive nanoscale coordination polymers enabling cancer combination therapy. *Biomaterials* **2017**, *146*, 40−48.

(8) Hu, C.-M. J.; Zhang, L. Nanoparticle-Based Combination Therapy toward Overcoming Drug Resistance in Cancer. *Biochem. Pharmacol.* **2012**, *83*, 1104−1111.

(9) Zheng, M.; Yue, C.; Ma, Y.; Gong, P.; Zhao, P.; Zheng, C.; Sheng, Z.; Zhang, P.; Wang, Z.; Cai, L. Single-Step Assembly of DOX/ICG Loaded Lipid−Polymer Nanoparticles for Highly Effective Chemo-photothermal Combination Therapy. *ACS Nano* **2013**, *7*, 2056.

(10) Li, Y.; Thambi, T.; Lee, D. S. Co-Delivery of Drugs and Genes Using Polymeric Nanoparticles for Synergistic Cancer Therapeutic Effects. *Adv. Healthcare Mater.* **2018**, *7*, 1700886.

(11) Pacardo, D. B.; Ligler, F. S.; Gu, Z. Programmable Nanomedicine: Synergistic and Sequential Drug Delivery Systems. *Nanoscale* **2015**, *7*, 3381−3391.

(12) Venkatesh, Y.; Rajesh, Y.; Karthik, S.; Chetan, A. C.; Mandal, M.; Jana, A.; Singh, N. D. P. Photocaging of Single and Dual (Similar or Different) Carboxylic and Amino Acids by Acetyl Carbazole and its Application as Dual Drug Delivery in Cancer Therapy. *J. Org. Chem.* **2016**, *81*, 11168−11175.

(13) Wong, P. T.; Tang, S.; Cannon, J.; Mukherjee, J.; Isham, D.; Gam, K.; Payne, M.; Yanik, S. A.; Baker, J. R.; Choi, S. K. A Thioacetal Photocage Designed for Dual Release: Application in the Quantitation of Therapeutic Release by Synchronous Reporter Decaging. *ChemBioChem* **2017**, *18*, 126−135.

(14) Chaudhuri, A.; Venkatesh, Y.; Behara, K. K.; Singh, N. D. P. Bimane: A Visible Light Induced Fluorescent Photoremovable Protecting Group for the Single and Dual Release of Carboxylic and Amino Acids. *Org. Lett.* **2017**, *19*, 1598−1601.

(15) Mitra, P.; Chakraborty, P. K.; Saha, P.; Ray, P.; Basu, S. Antibacterial efficacy of acridine derivatives conjugated with gold Nanoparticles. *Int. J. Pharm.* **2014**, *473*, 636−643.

(16) Zawada, Z.; Šafařík, M.; Dvořáková, E.; Janoušková, O.; Březinová, A.; Stibor, I.; Holada, K.; Bouř, P.; Hlaváček, J.; Šebestík, J. Quinacrine reactivity with prion proteins and prion-derived peptides. *Amino Acids* **2013**, *44*, 1279−1292.

(17) Belmont, P.; Bosson, J.; Godet, T.; Tiano, M. Acridine and acridone derivatives, anticancer properties and synthetic methods: where are we now? *Anti-Cancer Agents Med. Chem.* **2007**, *7*, 139−169.

(18) Denny, WA Acridine derivatives as chemotherapeutic agents. *Curr. Med. Chem.* **2002**, *9*, 1655−1665.

(19) Cholewiński, G.; Dzierzbicka, K.; Kołodziejczyk, A. M. Natural and synthetic acridines/acridones as antitumor agents: their biological activities and methods of synthesis. *Pharmacol. Rep.* **2011**, *63*, 305−336.

(20) Ferguson, L. R.; Denny, W. A. The genetic toxicology of acridines. *Mutation Research/Reviews in Genetic Toxicology* **1991**, *258*, 123−160.

(21) Chen, Y. Y.; Lukka, P. B.; Joseph, W. R.; Finlay, G. J.; Paxton, J. W.; McKeage, M. J.; Baguley, B. C. Selective cellular uptake and retention of SN 28049, a new DNA-binding topoisomerase II-directed antitumor agent. *Cancer Chemother. Pharmacol.* **2014**, *74*, 25−35.

(22) Zhuang, H.-B.; Tang, W.-J.; Yu, J.-Y.; Song, Q.-H. Acridin- 9-ylmethoxycarbonyl (Amoc): a new photochemically removable protecting group for alcohols. *Chin. J. Chem.* **2006**, *24*, 1465−1468.

(23) Piloto, A. M.; Hungerford, G.; Costa, S. P. G.; Gonçalves, M. S. T. Acridinyl methyl esters as photoactive precursors in the release of neurotransmitter amino acids. *Photochem. Photobiol. Sci.* **2013**, *12*, 339−347.

(24) Jana, A.; Saha, B.; Karthik, S.; Barman, S.; Ikbal, M.; Ghosh, S. K.; Pradeep Singh, N. D. Fluorescent Photoremovable precursors (acridin-9-ylmethyl)ester: Synthesis, Photophysical, Photochemical

and Biological applications. *Photochem. Photobiol. Sci.* **2013**, *12*, 1041−1052.
(25) Chaudhuri, A.; Paul, A.; Sikder, A.; Pradeep Singh, N. D. Single component photoresponsive fluorescent organic Nanoparticles: a smart platform for improved biomedical and agrochemical applications. *Chem. Commun.* **2021**, *57*, 1715−1733.
(26) Jana, A.; Devi, K. S. P.; Maiti, T. K.; Singh, N. D. P. Perylene-3-ylmethanol: Fluorescent Organic Nanoparticles as a Single-Component Photoresponsive Nanocarrier with Real-Time Monitoring of Anticancer Drug Release. *J. Am. Chem. Soc.* **2012**, *134*, 7656−7659.
(27) Jana, A.; Saha, B.; Banerjee, D. R.; Ghosh, S. K.; Nguyen, K. T.; Ma, X.; Qu, Q.; Zhao, Y.; Singh, N. D. P. Photocontrolled Nuclear-Targeted Drug Delivery by Single Component Photoresponsive Fluorescent Organic Nanoparticles of Acridin-9-Methanol. *Bioconjugate Chem.* **2013**, *24*, 1828−1839.
(28) Biswas, S.; Das, J.; Barman, S.; Rao Pinninti, B.; K. Maiti, T.; Singh, N. D. P. Environment Activatable Nanoprodrug: Two-Step Surveillance in the Anticancer Drug Release. *ACS Appl. Mater. Interfaces* **2017**, *9*, 28180−28184.
(29) Biswas, S.; Mengji, R.; Barman, S.; Venugopal, V.; Jana, A.; Singh, N. D. P. 'AIE + ESIPT' assisted photorelease: fluorescent organic nanoparticles for dual anticancer drug delivery with real-time monitoring ability. *Chem. Commun.* **2018**, *54*, 168−171.
(30) Blaheta, R. A.; Michaelis, M.; Driever, P. H.; Cinatl, J. Evolving Anticancer Drug Valproic Acid: Insights into the Mechanism and Clinical Studies. *Med. Res. Rev.* **2005**, *25*, 383−397.
(31) Kasai, H.; Oikawa, H.; Okada, S.; Nakanishi, H. Crystal Growth of Perylene Microcrystals in the Reprecipitation Method. *Bull. Chem. Soc. Jpn.* **1998**, *71*, 2597−2601.
(32) Al-Kaysi, R. O.; Müller, A. M.; Ahn, T.-S.; Lee, S.; Bardeen, C. J. Effects of Sonication on the Size and Crystallinity of Stable Zwitterionic Organic Nanoparticles Formed by Reprecipitation in Water. *Langmuir* **2005**, *21*, 7990−7994.
(33) Carole, D. G.; Michel, D. M.; Julien, C.; Florence, D.; Anna, N.; Séverine, J.; Gérard, D.; Pierre, T.-D.; Jean-Pierre, G. Synthesis and antileishmanial activities of 4,5-di-substituted acridines as compared to their 4-mono-substituted homologues. *Bioorg. Med. Chem.* **2005**, *13*, 5560−5568.
(34) Fletcher, A. N. Quinine sulfate as a fluorescence quantum yield standard. *Photochem. Photobiol.* **1969**, *9*, 439−444.
(35) Demas, J. N.; Bowman, W. D.; Zalewski, E. F.; Velapoldi, R. A. Determination of the Quantum Yield of the Ferrioxalate Actinometer with Electrically Calibrated Radiometers. *J. Phys. Chem.* **1981**, *85*, 2766−2771.
(36) Ikbal, M.; Saha, B.; Barman, S.; Atta, S.; Banerjee, D. R.; Ghosh, S. K.; Singh, N. D. P. Benzo[a]acridinyl methyl esters as pH Sensitive Fluorescent Photoactive precursors: Synthesis, Photophysical, Photochemical and Biological Applications. *Org. Biomol. Chem.* **2014**, *12*, 3459−3469.
(37) Sikder, A.; Banerjee, M.; Singha, T.; Mondal, S.; Datta, P. K.; Anoop, A.; Singh, N. D. P. A Natural Alkaloid, ß-Carboline, as a One- and Two-Photon Responsive Fluorescent Photoremovable Protecting Group: Sequential Release of the Same or Different Carboxylic Acids. *Org. Lett.* **2020**, *22*, 6998−7002.
(38) Kalyane, D.; Raval, N.; Maheshwari, R.; Tambe, V.; Kalia, K.; Tekade, R. K. Employment of enhanced permeability and retention effect (EPR): Nanoparticle-based precision tools for targeting of therapeutic and diagnostic agent in cancer. *Mater. Sci. Eng., C* **2019**, *98*, 1252−1276.
(39) Chen, J.; Ghazawi, F. M.; Bakkar, W.; Li, Q. Valproic acid and butyrate induce apoptosis in human cancer cells through inhibition of gene expression of Akt/protein kinase B. *Mol. Cancer* **2006**, *5*, 71.
(40) Heers, H.; Stanislaw, J.; Harrelson, J.; Lee, M. W. Valproic acid as an adjunctive therapeutic agent for the treatment of breast cancer. *Eur. J. Pharmacol.* **2018**, *835*, 61−74.

https://doi.org/10.1021/acsanm.2c01515
ACS Appl. Nano Mater. 2022, 5, 7512−7520